

# Performance and mechanism of sand stabilization via microbial-induced CaCO<sub>3</sub> precipitation using phosphogypsum

Hao Bao<sup>a,b,c</sup>, Zhaoran Zheng<sup>b</sup>, Gang Xu<sup>a,b,\*</sup>, Rende Li<sup>b</sup>, Qing Wang<sup>a,b</sup>, Mohamed Saafi<sup>c</sup>, Jianqiao Ye<sup>c</sup>

- a. Hubei Key Laboratory of Disaster Prevention and Mitigation, China Three Gorges University, Yichang, China  
b. College of Civil Engineering & Architecture, China Three Gorges University, Yichang, China  
c. Department of Engineering, Lancaster University, Lancaster LA1 4YR, UK

\* Correspondence author: postxg@163.com (G. Xu)

**Abstract:** Phosphogypsum is a solid waste generated during the production of phosphoric acid. Effective utilization of phosphogypsum resources is a complex challenge. In this research, an innovative and eco-friendly sand consolidation technique, i.e., microbial-induced CaCO<sub>3</sub> precipitation using phosphogypsum (MICPP), is applied to achieve phosphogypsum mineralization and sand stabilization. Phosphogypsum is employed as a calcium source for sand consolidation. To elucidate the efficiency and the mechanism of sand consolidation through MICPP, a series of experimental tests on the sand columns using varying phosphogypsum dosages and consolidation methods are conducted. The results show a positive correlation between the increase in phosphogypsum dosage and the increase in the compressive strength of the specimens. Concurrently, As the amount of phosphogypsum increased, the permeability coefficient of the sand columns decreased and the production of CaCO<sub>3</sub> increased. Notably, the immersion method exhibits a superior curing effect compared to the stirring method. The MICPP-treated specimens significantly mitigated the risk of environmental contamination. The CaCO<sub>3</sub> precipitated by the microbial action is predominantly in the form of calcite that effectively fills the voids, bond surfaces, and bridge gaps in the sand columns, thereby substantially enhancing the performance of sand columns.

**Keywords:** Sand stabilization, MICPP, Performance evaluation, Mechanistic analysis, Environmental assessment.

## 1. Introduction

In the context of global warming, a range of measures have been actively implemented by many countries to reduce greenhouse gas emissions, including CO<sub>2</sub> [1]. Traditional soil reinforcement techniques rely on cementitious materials [2-4]. However, the use of conventional reinforcing agents like cement and lime alters the pH of soil, induces alkalinity and creates erosive conditions, which negatively impacts groundwater and surrounding vegetation [5]. Additionally, substantial CO<sub>2</sub> emissions generated during the production of cement, upon which this technology heavily relies, hinder progress toward the carbon reduction targets [6-8]. Recently, Microbially Induced Calcium Carbonate Precipitation (MICP) technology is gaining prominence due to its environmentally friendly, efficient, controllable, and cost-effective attributes, coupled with low energy consumption and sustainability [3, 9, 10]. MICP operates on the principle of utilizing microorganisms to decompose urea into carbonate ions. Subsequently, these ions combine with

41 calcium ions, forming  $\text{CaCO}_3$  precipitation and exerting a curing effect <sup>[11]</sup>. The technology holds  
42 significant promises across various civil engineering applications, including foundation  
43 reinforcement <sup>[3, 12-15]</sup>, crack repair, overlay applications <sup>[16-19]</sup>, soil heavy metal management <sup>[20, 21]</sup>,  
44 soil permeability enhancement <sup>[22, 23]</sup>, slope stabilization, and soil erosion control <sup>[24]</sup>. The diverse  
45 applications underscore the potential of MICP to positively impact the sustainable evolution of the  
46 civil engineering sector.

47 The concept of MICP involves injecting bacteria and cementing solution through alternating  
48 grouting cycles to carry out one-dimensional sand column reinforcement <sup>[25]</sup>. This process notably  
49 increases the strength of the column. The mechanism behind microbial-induced  $\text{CaCO}_3$   
50 precipitation relies on the urea hydrolysis reaction and involves the enzymatic activity of urease-  
51 producing bacteria, which continually decomposes urea. As a result,  $\text{NH}_4^+$  is released, elevating  
52 the micro environmental alkalinity. Consequently, continuous  $\text{CO}_2$  absorption and conversion into  
53  $\text{CO}_3^{2-}$  occur, facilitating its combination with  $\text{Ca}^{2+}$  from the calcium source, leading to the  
54 precipitation of  $\text{CaCO}_3$  <sup>[20,26,27]</sup>. Compressive strength is a crucial parameter characterizing the  
55 strength properties of MICP curing. Observations of compressive strength and calcite deposition  
56 demonstrated a marked improvement in strength correlated with increased calcite deposition <sup>[3, 28-</sup>  
57 <sup>30]</sup>. Moreover, MICP treatment results in varied enhancements of cohesion ( $c$ ) and the angle of  
58 internal friction ( $\phi$ ) in the treated specimens, thereby boosting the shear strength of sandy soil  
59 <sup>[31,32]</sup>. Calcium carbonate precipitation induced by MICP fills granular soil pores, potentially  
60 enhancing soil porosity, and permeability, and enabling the sealing of porous materials <sup>[33,34]</sup>.  
61 Ongoing studies utilize calcium chloride, calcium acetate, and calcium nitrate as primary calcium  
62 sources, while alternative sources like concentrated seawater, calcium gluconate, calcium lactate,  
63 and even eggshells are explored <sup>[27,35-38]</sup>.

64 The surging expansion of the phosphate industry aligns with the swift growth of agricultural  
65 industry. Phosphogypsum constitutes a considerable solid waste residue, emanating as a  
66 byproduct from the production of wet phosphoric acid. Present estimations unveil a significant  
67 worldwide accrual of phosphogypsum, averaging 4.5-5.5 tons for every ton of produced  
68 phosphoric acid <sup>[39, 40]</sup>. Regrettably, a majority of phosphogypsum is disposed in stockpiles or  
69 landfills, with limited application in specialized sectors such as construction materials and  
70 fertilizer production. This practice poses significant challenges to both environmental  
71 sustainability and resource management <sup>[41]</sup>. Consisting primarily of calcium sulfate dihydrate  
72 ( $\text{CaSO}_4 \cdot 2\text{H}_2\text{O}$ ) <sup>[42]</sup>, researchers have dissolved phosphogypsum using alkaline solutions.  
73 Subsequent experiments involving carbonization at room temperature and pressure have  
74 demonstrated high efficiency in producing  $\text{CaCO}_3$  precipitates. Further exploration shows

75 complete transfer of trace elements from phosphogypsum waste to the resulting calcite precipitate  
76 <sup>[43]</sup>. At present, MICP technology is rapidly advancing and reaching a state of maturity. However,  
77 there is a lack of research focusing on the utilization of phosphogypsum as a calcium source in  
78 MICP. This study introduces an innovative approach by utilizing phosphogypsum as a calcium  
79 source within the framework of MICP technology. Through the action of microbial processes,  
80 phosphogypsum undergoes transformation into a viable material suitable for engineering  
81 applications, which is termed microbial-induced calcium carbonate precipitation using  
82 phosphogypsum (MICPP). As shown in Fig. 1, an initiative is directed towards providing a  
83 sustainable pathway for the utilization of phosphogypsum resources, with the potential to alleviate  
84 phosphogypsum accumulation and mitigate environmental stress, as well as to utilize  
85 phosphogypsum as a source of calcium in MICPP, which also offers economic benefits of this  
86 technology. Nevertheless, phosphogypsum exhibits a more acidic nature, featuring a pH range of  
87 approximately 2-5 <sup>[44]</sup>, diverging from the alkaline environments favorable for urease-producing  
88 bacteria typically employed in MICP <sup>[45]</sup>, which may hinder the viability and metabolic functions  
89 of bacteria within phosphogypsum substrates. However, as a nutrient source, urea undergoes  
90 hydrolysis to produce  $\text{CO}_3^{2-}$  and  $\text{NH}_4^+$ , consequently increasing the pH and creating an optimal  
91 environment for bacterial proliferation. This, in turn, enhances bacterial activity in  
92 phosphogypsum solutions.

93 In this investigation, unconfined compressive strength tests and impermeability assessments  
94 are conducted to evaluate the macroscopic properties of the sands stabilized by MICPP.  
95 Additionally, leaching analyses are executed to assess the potential environmental impact of the  
96 specimens in terms of detected hazardous elements. Scanning Electron Microscope (SEM) and X-  
97 ray Diffractometer (XRD) are employed for microscopic examinations of the treated specimens.  
98 Furthermore, the generated  $\text{CaCO}_3$  is quantified. The use of both macroscopic and microscopic  
99 analyses aims to comprehensively understand the macroscopic attributes and reinforcement  
100 mechanisms linked with MICPP-treated sands. Ultimately, our findings aim to provide valuable  
101 insights and guidance for the advancement and practical implementation of the MICPP technology  
102 utilizing phosphogypsum as a calcium source.

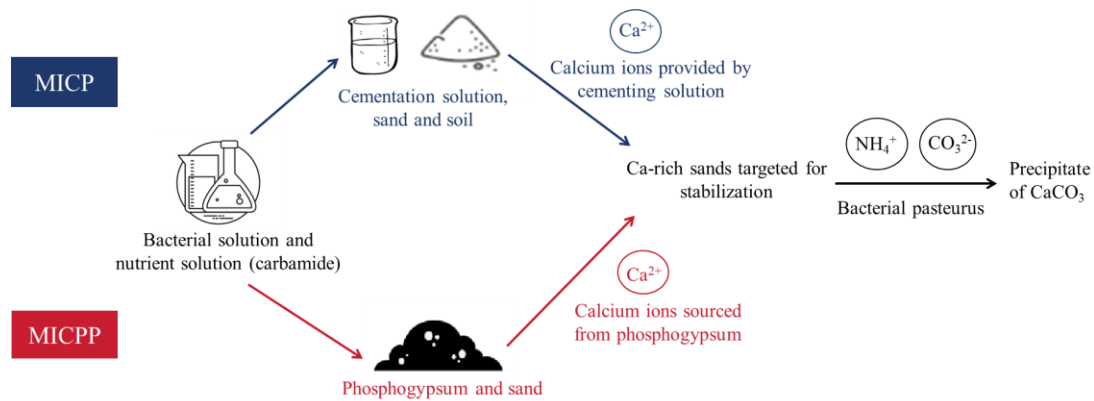


**Fig. 1.** Flowchart of the incumbent mineralization process of MICP (blue) and the proposed mineralization process of phosphogypsum (red) for sand stabilization using MICPP.

## 103 2. Test materials and experimental schemes

### 104 2.1. Materials and reagents

#### 105 2.1.1. Phosphogypsum and sands

106 The phosphogypsum originated from Yichang, China, of which the primary constituent is  
 107  $\text{CaSO}_4 \cdot 2\text{H}_2\text{O}$ , displaying a dark gray color. The pH measurement is approximately in the range of  
 108 4.0-5.0. The content analysis shows a calcium sulfate dihydrate concentration of 89.23%.  
 109 Phosphogypsum also contains impurities, including phosphorus, fluorine, and organic matter. The  
 110 chemical composition of the untreated phosphogypsum is detailed in Table 1.

111 **Table 1**

112 Chemical composition of phosphogypsum (%).

$\text{SO}_3$	CaO	$\text{SiO}_2$	$\text{Fe}_2\text{O}_3$	$\text{P}_2\text{O}_5$	$\text{Al}_2\text{O}_3$	$\text{K}_2\text{O}$	BaO	SrO	TiO	CuO
51.40	36.11	8.98	0.68	0.59	0.57	0.56	0.47	0.38	0.24	0.02

113 Table 2 provides the fundamental physical characteristics of the river sands. Fig. 2 illustrates  
 114 the particle grading curve of the sands subjected to testing. The sands exhibit a fineness modulus  
 115 of 1.05, classified as fine sands.

116 **Table 2**

117 The physical properties of sands.

Water content (%)	Apparent density ( $\text{g}/\text{cm}^3$ )	Bulk density ( $\text{g}/\text{cm}^3$ )	Void fraction (%)
0	2.66	1.54	46.35

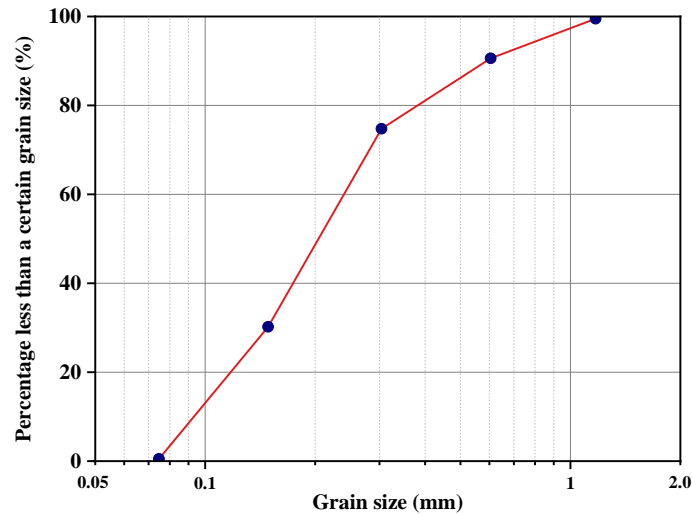


**Fig. 2.** Particle grading curve of test sands.

118 *2.1.2. Activation and cultivation of bacteria*

119 The chosen bacterial strain for this experimental investigation is *Bacillus pasteurii*, a Gram-  
 120 positive bacillus ubiquitously present in diverse environmental matrices, including soil, water, and  
 121 air. *Bacillus* species exhibit robust metabolic capabilities, environmental benignity, and high  
 122 urease activity. The strain used in this study is *Bacillus pasteurii* (GDMCC 1.083) from  
 123 Guangdong Microbial Culture Collection Center. In the experimental procedure, a liquid medium  
 124 with a composition detailed in Table 3 was utilized.

125 **Table 3**

126 Ratio per L of liquid medium.

Reagents	Content of liquid medium components
Casein Peptone	15g
Soy Peptone	5g
NaCl	5g
Urea	20g
Distilled Water	1L

127 The activated bacterial solution is introduced to the liquid medium at a volumetric ratio of  
 128 1:50. In particular, 10 ml of the bacterial solution is carefully pipetted into a conical flask  
 129 containing 500 ml of sterile liquid medium. Subsequently, the mixture is placed in a constant-  
 130 temperature shaking incubator set at 30°C and agitated at a speed of 120 rpm for a duration of 48  
 131 hours. The spectrophotometer is employed to assess the OD600 value of the bacterial solution.  
 132 OD600 serves as a standardized method for quantifying microbial growth in liquid media,  
 133 characterizing bacterial concentration based on the absorbance of solution at a wavelength of 600  
 134 nm. Urea undergoes hydrolysis into  $\text{NH}_4^+$  and  $\text{CO}_3^{2-}$  during metabolic processes, catalyzed by the  
 135 urease produced by *Bacillus pasteurianus*. The resultant metabolic change influences the  
 136 conductivity within the reaction system, enabling an evaluation of bacterial activity through

137 variations in electrical conductivity (EC). The formula for calculating urease activity is shown in  
138 Eq. (1) <sup>[25]</sup>. Urease activity is quantified at around 8 mmol/(L×min) using a conductivity meter.

$$(1)$$

139 where:  $A$  represents urease activity in mmol/(L×min);  $E$  denotes conductivity in ms/cm;  $t$  is time  
140 in minutes; and  $n$  denotes dilution.

141 To elucidate the influence of the *Bacillus pasteurianus* metabolic activities on the pH  
142 dynamics of the growth medium, pH measurements of the liquid medium are taken throughout  
143 bacterial cultivation, aiming to observe the pH trends and interpret the bacterial adaptation  
144 mechanisms. Fig. 3 illustrates the temporal evolution of the pH value of the bacterial solution. It  
145 is evident that the bacterial solution reaches full maturation with its pH stabilizing between 9 to  
146 9.5.

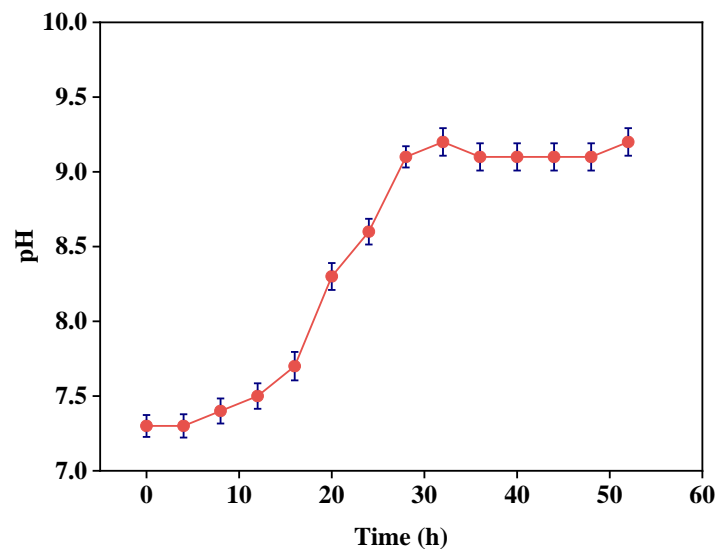


**Fig. 3.** pH value of the bacterial solution over time.

147 The MICPP reaction is a multifaceted process governed by many influencing factors.  
148 Assessing  $\text{Ca}^{2+}$  conversion rate is pivotal for the effective application of the MICPP technique.  
149 Preliminary experiments are conducted then to ascertain the  $\text{Ca}^{2+}$  conversion rate prior to  
150 commencing the formal experiments. The  $\text{Ca}^{2+}$  conversion rate is defined as the proportion of the  
151 mass of  $\text{Ca}^{2+}$  incorporated into the calcium carbonate precipitate produced through MICPP to the  
152 initial mass of  $\text{Ca}^{2+}$  in the calcium source. Fig. 4 illustrates the temporal evolution of  $\text{Ca}^{2+}$   
153 conversion for various calcium source solutions, with the  $\text{Ca}^{2+}$  conversion ultimately determined  
154 to be approximately 80%. Despite that phosphogypsum has a lower  $\text{Ca}^{2+}$  conversion rate  
155 compared to other calcium sources, the 80%  $\text{Ca}^{2+}$  conversion rate, as shown in Fig. 4, is  
156 undoubtedly noteworthy.

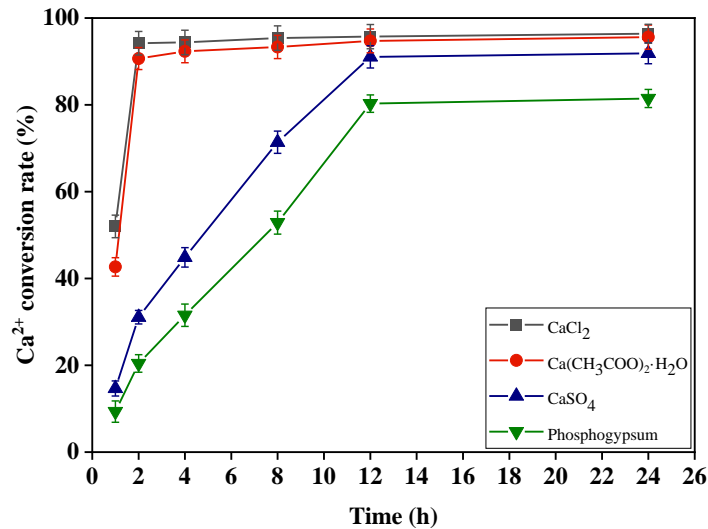


**Fig. 4.** Curve of Ca<sup>2+</sup> conversion rate over time.

157 As shown also in Fig. 4, the initial phase of the MICPP reaction manifests a diminished Ca<sup>2+</sup>  
 158 conversion rate. This phenomenon can be attributed to the initially acidic pH value of the solution,  
 159 indicative of subdued bacterial activity. With the advancement of the reaction, the hydrolysis of  
 160 urea becomes more pronounced, resulting in a substantial augmentation in the generation of CO<sub>3</sub><sup>2-</sup>  
 161 and NH<sub>4</sub><sup>+</sup>. The elevation in pH value creates an optimal milieu for bacterial proliferation,  
 162 consequently amplifying bacterial activity within the phosphogypsum solution.

## 163 **2.2. Preparation of sand columns**

164 Two distinct curing methods are applied in the preparation of the sand columns: (1) Stirring  
 165 Method: In accordance with the predetermined ratios, the sand sample and phosphogypsum are  
 166 accurately weighed and subsequently blended with the bacterial solution and a 1 mol/L urea  
 167 nutrient solution. This mixture is then thoroughly stirred prior to its introduction into the mold to  
 168 formulate the sand column. (2) Immersion Method: The sand sample and phosphogypsum are  
 169 weighed based on the pre-established proportions, thoroughly amalgamated, and subsequently  
 170 introduced into the mold to create the sand column. Following this, the column is submerged in a  
 171 nutrient solution comprising bacterial solution and 1 mol/L urea for ongoing maintenance. The  
 172 flow chart for the preparation of the sand columns is shown in Fig. 5. The mold is a PVC pipe  
 173 with an inner diameter of 4.8 cm and a height of 5 cm that is sterilized to eliminate potential  
 174 interference with experimental results by external impurities. In the process of preparing the  
 175 specimens, a layer of petroleum jelly is initially applied to the inner wall of the PVC pipe to  
 176 facilitate the subsequent demolding of the specimens. A layered filling process is followed,  
 177 ensuring that each layer undergoes proper vibration and compaction. All the materials utilized in  
 178 the experiments, including the sand samples, bacterial fluid, and phosphogypsum, are measured  
 179 for the predefined proportions and thoroughly mixed through adequate agitation. Following the

180 preparation stage, the specimens are subjected to a curing period of 7 days, followed by a drying  
 181 phase at 60°C for 48 hours. Following the preparation stage, the specimens undergo a curing  
 182 period of 7 days, followed by a drying phase at 60°C for 48 hours.

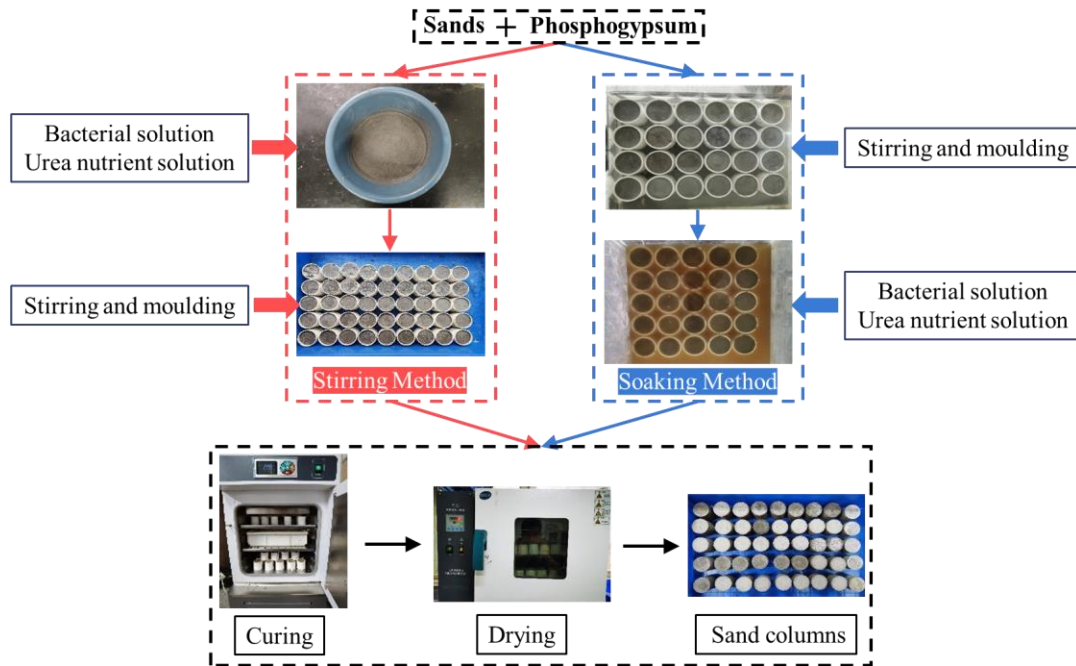


Fig. 5. Flow chart for the preparation of sand columns.

183 **2.3. Experiment design**

184 After the curing process, the sand columns are tested to evaluate the unconfined compressive  
 185 strength, impermeability, and leaching of the specimens. Following that, evaluations are carried  
 186 out on the CaCO<sub>3</sub> generation and microstructural properties of the specimens, under different  
 187 curing conditions, with the aim of uncovering micro-mechanisms. The combination of  
 188 macroscopic observations and micro-mechanical insights shows the inherent reinforcement  
 189 mechanism. The details of the experiments for microbial-induced CaCO<sub>3</sub> precipitation using  
 190 phosphogypsum and the microstructure analysis adhered to the standardized experimental design,  
 191 are shown in Table 4.

192 **Table 4**

193 Experimental design.

Groups	Bacterial solution (OD <sub>600</sub> )	Phosphogypsum (g)	Sand (g)
BSP-20	1.5	26	104
BSP-40		52	78
BSP-60		78	52
BSP-80		104	26
BSP-100		130	0
SP-20	0	26	104
SP-40		52	78
SP-60		78	52
SP-80		104	26
SP-100		130	0

BIP-20		26	104
BIP-40		52	78
BIP-60	1.5	78	52
BIP-80		104	26
BIP-100		130	0
IP-20		26	104
IP-40		52	78
IP-60	0	78	52
IP-80		104	26
IP-100		130	0

194 Note: *B* represents use of bacterial solutions; *P* denotes the addition of phosphogypsum; *S* and *I* indicate the  
195 stirring method and immersion method, respectively. The numbers in groups represent the percentage of  
196 phosphogypsum admixture.

## 197 **2.4. Experimental methods**

### 198 *2.4.1. Unconfined compressive strength*

199 Consistent with the well-established methodologies in sand reinforcement assessment,  
200 unconfined compressive strength is one of the primary properties in evaluating sand strength after  
201 microbial-induced CaCO<sub>3</sub> precipitation using phosphogypsum. The strength of the material is  
202 evaluated by gradually applying axial pressure until the specimen ruptured, and the maximum of  
203 the applied pressure is then deemed as the unconfined compressive strength. The unconfined  
204 compressive strength is evaluated for different amounts of phosphogypsum and curing methods.  
205 To mitigate potential testing errors, the upper and lower surfaces of the specimens are carefully  
206 sanded prior to the testing. Three independent specimens of each set of ratios are made and tested  
207 to ensure consistency. The compressive load is applied uniformly in the direction of compression.  
208 The specimen is placed on the lifting table of the WAW-Y1000C Universal Testing Machine and  
209 loaded at a rate of 1 mm/min.

### 210 *2.4.2. Permeability*

211 Owing to the filling of the pore spaces by the products of microbial mineralization reactions  
212 and the cementation of sand particles, a substantial reduction in the permeability coefficient is  
213 observed in comparison to that of the pre-reinforcement state. The variable head test method is  
214 used to evaluate this reduction. Eq. (2) is the equation used in the variable head permeability test  
215 to calculate the permeability coefficient of sand columns<sup>[46]</sup>.

$$k = 2.3 \frac{aL}{At} \lg \frac{H_1}{H_2} \quad (2)$$

216 where, *k* represents permeability coefficient (cm/s); *a* signifies cross-sectional area of the variable  
217 head pipe (cm<sup>2</sup>); *L* denotes path of penetration, i.e., the height of the specimen (cm); *H*<sub>1</sub> represents  
218 the head at the start (cm); *H*<sub>2</sub> signifies the head at termination (cm); *t* represents time (s); and *A*  
219 signifies cross-sectional area (cm<sup>2</sup>).

### 220 *2.4.3. Determination of CaCO<sub>3</sub> content*

221 To accurately quantify the  $\text{CaCO}_3$  content generated within the sand column during  
 222 microbial-induced  $\text{CaCO}_3$  precipitation using phosphogypsum, a custom-designed testing system  
 223 (Fig. 6) is employed. This system facilitates the determination of  $\text{CaCO}_3$  content by subjecting it  
 224 to dilute hydrochloric acid within the sand column, triggering the release of carbon dioxide gas in  
 225 accordance with the principles of the Carbonate Content Test Method. The  $\text{CaCO}_3$  content is  
 226 dependent of the air pressure and the formula calculates the percentage of  $\text{CaCO}_3$  content ( $W$ ), as  
 227 shown in Eq. (3) <sup>[47]</sup>.

$$W = \frac{PVM}{RTm} \times 100\% \quad (3)$$

228 where  $P$  represents the measured air pressure in pascals (Pa);  $V$  signifies the volume of generated  
 229  $\text{CO}_2$  gas;  $M$  denotes the molar mass of  $\text{CaCO}_3$  in grams per mole (g/mol);  $R$  is the gas constant,  
 230 having a standard value of  $8.314 \text{ J}/(\text{K}\cdot\text{mol})$ ;  $T$  is the gas temperature within the device, measured  
 231 in Kelvin (K), where  $0^\circ\text{C}$  is equivalent to  $273.15\text{K}$ ; and  $M$  signifies the mass of the specimen  
 232 powder in grams (g).



**Fig. 6.** Micro-precision digital carbonation measuring instrument.

#### 233 2.4.4. Leaching test for harmful elements

234 At elevated concentrations, fluoride, a prevalent groundwater contaminant, presents potential  
 235 health hazards. Water acidity or alkalinity, which may profoundly influence the aquatic ecosystem,  
 236 is dependent on pH. Leaching tests are conducted by dissolving phosphogypsum in water, where  
 237 the soluble contaminants are dissolved and diffused into the leaching solution, and the amount of  
 238 soluble contaminants in the leaching solution is measured. The objective of this process is to  
 239 ascertain concentration of pollutants in the leaching solution, appraise the harmful characteristics  
 240 of the waste, and assess its environmental impact. In this study, the standards for water pH  
 241 determination (HJ 1147-2020) <sup>[48]</sup> and ion-selective electrode method (GB/T 7484-1987) <sup>[49]</sup> are  
 242 strictly followed. The chosen leaching agent is deionized water, and its volume is determined to  
 243 achieve a liquid-to-solid ratio of 10:1.

#### 244 2.4.5 Microscopic analysis

245 The  $\text{CaCO}_3$ , formed primarily via microbial-induced  $\text{CaCO}_3$  precipitation using  
 246 phosphogypsum, exhibits properties described by its crystalline structure and morphology. In  
 247 conducting the microstructural examinations, a JSM-7500F scanning electron microscope  
 248 manufactured by Nihon Electronics is used to provide magnification in the order of tens of  
 249 thousands of times. Furthermore, qualitative analysis of the specimens is conducted using a  
 250 SmartLab X-ray diffractometer manufactured by Nippon Rigaku. This facilitates a comparison of  
 251 the compositions between the MICPP treated specimens and their untreated counterparts.

### 252 3. Results and discussion

#### 253 3.1. Unconfined compressive strength of stabilized sands

##### 254 3.1.1. Effect of phosphogypsum dosage

255 The unconfined compressive strength of the specimens, prepared using two curing methods  
 256 (stirring and immersion), for different phosphogypsum dosages, is illustrated in Fig. 7. The  
 257 compressive strength of the sand columns increases gradually with the increase of the amount of  
 258 phosphogypsum. In the absence of microbial induction, the unconfined compressive strength of  
 259 sand columns is about 0.1 MPa at 20% dosage. However, with the use of MICPP, the strength of  
 260 the specimens prepared using the stirring method increases to 0.4 MPa, while the strength of the  
 261 specimens prepared using the immersion method increases to 0.63 MPa. The compressive strength  
 262 of the sand columns manufactured through immersion surpasses that of the columns manufactured  
 263 through mixing by 57.5%. With an 80% phosphogypsum dosage, the stirring method yields a  
 264 compressive strength of 0.98 MPa, while the immersion method results in 1.19 MPa. These  
 265 findings are consistent with previous studies on sand treated with MICP, as summarized in Table 5  
 266 [50]. The results illustrate a significant improvement induced by MICPP technology in  
 267 phosphogypsum mineralization. Nevertheless, with a 100% phosphogypsum dosage, the  
 268 unconfined compressive strength does not increase significantly from that of the specimens with  
 269 an 80% dosage.

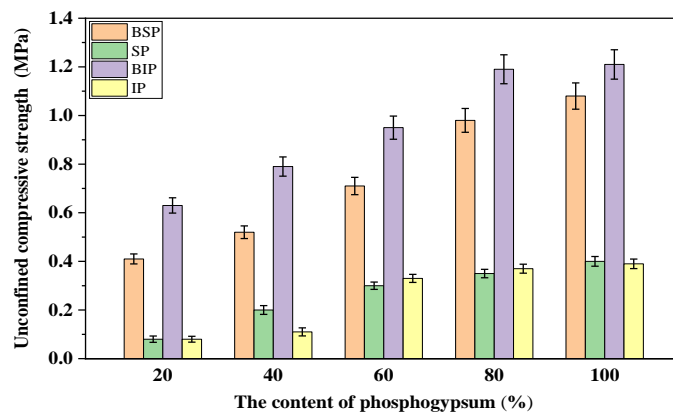


**Fig. 7.** Unconfined compressive strength of specimens at various phosphogypsum dosages.

270  
271

**Table 5**

Previous studies on the unconfined compressive strength of MICP-treated sand.

Bacteria Name	Sand		Density (g/cm <sup>3</sup> )	Compressive strength (MPa)	Reference
	Urease activity	Type			
Sporosarcina pasteurii	0.23 mS/min	Itterbeck sand	1.56	0.19-0.574	[30]
Sporosarcina pasteurii	0.8-1.2 (OD600)	British sand	0.2-1.0	0.37-2.95	[51]
Bacillus sphaericus	10 U/ml	Ottawa sand	1.62-1.63	0.180-2.27	[52]
S. pasteurii and urease	0.3-1.5 (OD600)	Ottawa sand	1.58-1.64	0.098-2.145	[53]
Bacillus sp.	10 U/ml	Silica sand	1.63-1.85	0.037-2.112	[54]
S. pasteurii	0.6-1.2 (OD600)	Xiamen sand	-	0.048-1.872	[55]

272 *3.1.2. Failure mode*

273 Fig. 8 illustrates the damage morphology of a representative specimen from the MICPP  
274 group. In the SP and IP specimens, the regions near the ends are more prone to loosening due to  
275 the relatively weak bonds, making them susceptible to initial damage under pressure. The lack of  
276 microbial-induced mineralization in these regions leads to structural weakness and the subsequent  
277 fracture under external loading, reducing the compressive strength of the samples and leading to  
278 severe fracture. The lack of effective calcium carbonate cementation, low cohesion between  
279 particles, and the insufficient internal friction angle to provide adequate resistance make these  
280 samples susceptible to structural loosening and cracking when subjected to compression.

281 In the MICPP-treated specimens (BSP and BIP), cracks gradually expand from the bottom to  
282 the top, displaying a typical shear failure mode with a distinct shear slip surface. This failure mode  
283 is primarily due to the non-uniform distribution of CaCO<sub>3</sub> precipitation in the spatial location,  
284 resulting in overall strength non-uniformity. Specifically, CaCO<sub>3</sub> precipitates increase gradually  
285 from the bottom to the top in the vertical direction, leading to a relatively low strength at the  
286 bottom of the sample and a higher strength at the top. Although the formation of CaCO<sub>3</sub> enhances  
287 cohesion and internal friction angle, improving overall stability and compressive resistance, the  
288 uneven distribution of CaCO<sub>3</sub> precipitates results in uneven strength, affecting the uniformity of  
289 the force in the material and the stress transfer under external loads. Particularly in the bottom  
290 regions with less precipitation, the lower cohesion and internal friction angle make these regions  
291 potential locations of damage initiation, further leading to the emergence of the distinct shear  
292 damage modes.

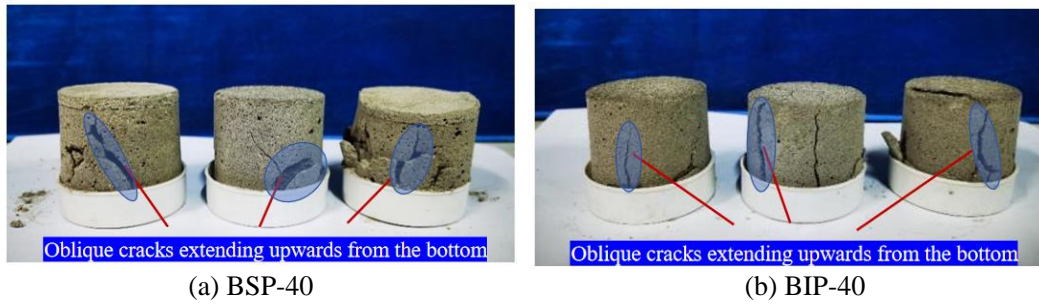


**Fig. 8.** Failure mode of sand columns.

293 **3.2. Permeability coefficient of stabilized sands**

294 The permeability coefficient ( $K$ ) acts as a crucial indicator for assessing sample permeability.  
 295 The variable head permeability test allows for a more accurate assessment of the influence of  
 296 MICPP products on the permeability of the specimens, providing crucial insights into the curing  
 297 process. As depicted in Fig. 9, various phosphogypsum dosages and sand curing methods have a  
 298 significant impact on the permeability. Initially, the original specimen has a permeability  
 299 coefficient of  $9.928 \times 10^{-4}$  cm/s, commonly associated with the pore structure of the sand columns.  
 300 Reduced and increased permeability coefficients are often associated with finer particles and  
 301 higher porosity, respectively. For example, The SP-20 and IP-20 sand columns have a decreased  
 302 permeability coefficient of around  $8.0 \times 10^{-4}$  cm/s. The minimum particle size of the river sands  
 303 used in the experiment is 0.1 mm, whereas the size of the phosphogypsum particles is smaller.  
 304 Consequently, the phosphogypsum particles effectively fill the gaps between the sand particles,  
 305 thereby reducing the permeability coefficient of the sand column. With microbial curing, the  
 306 permeability coefficient decreases to  $8.954 \times 10^{-5}$  cm/s, representing a substantial magnitude of  
 307 improvement. Particularly, the specimens treated through immersion exhibited an 18%  
 308 improvement compared to those treated through agitation. At an 80% phosphogypsum dosage,  
 309 the specimens cured through stirring have a decreased permeability coefficient of  $5.901 \times 10^{-5}$  cm/s.  
 310 However, it is observed that adding any additional phosphogypsum improves permeability only  
 311 marginally. The immersion-treated group with 80% phosphogypsum shows a permeability  
 312 coefficient of  $4.089 \times 10^{-5}$  cm/s, signifying an almost 50% improvement in impermeability  
 313 compared to the stirring method. These observations align with the outcomes of existing research  
 314 on MICP-treated sand, as shown in Table 6 <sup>[50]</sup>. Overall, MICPP can significantly enhance  
 315 impermeability, particularly, when the immersion method is used.

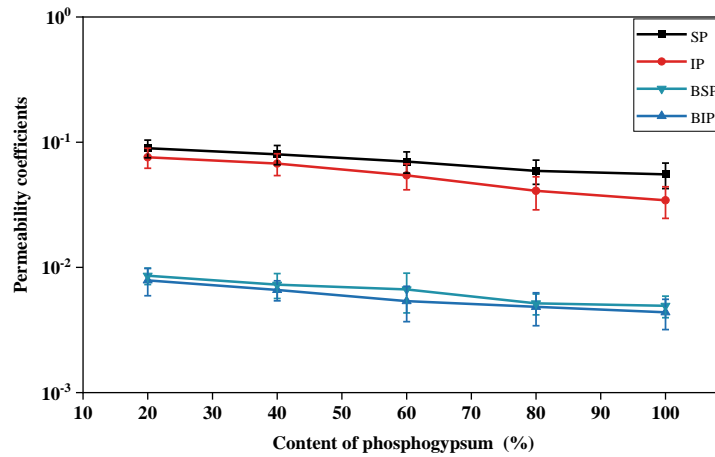


**Fig. 9.** Permeability coefficients of specimens with varied phosphogypsum dosages.

316 **Table 6**

317 Previous studies on permeability of MICP-treated sands.

Bacteria	Soil		Permeability	Reference
Name	Urease activity	Type	Density (g/cm <sup>3</sup> ) (m/s)	
Sporosarcina pasteurii	0.8 to 1.2 (OD600)	British sand	0.2 to 1.0 (R.D) 1.18×10 <sup>-6</sup>	[51]
Bacillus sp.	10 U/ml	Silica sand (Australia)	1.60 to 1.61 4.22×10 <sup>-5</sup>	[52]
Sporosarcina pasteurii	3.7 mM/min	Ottawa sand	1.65 1.16×10 <sup>-5</sup>	[56]
Sporosarcina pasteurii	0.8 to 1.2 (OD600)	Sand	- 2.54×10 <sup>-6</sup>	[57]

318 **3.3. Assessment of CaCO<sub>3</sub> production**

319 The quality of CaCO<sub>3</sub> deposition within a specimen is a crucial indicator when assessing the  
 320 effectiveness of the MICPP technology. It not only reflects the quality of mineralization but also  
 321 serves as the foundation for optimizing MICPP process parameters, thereby enhancing curing  
 322 efficiency and effectiveness. As illustrated in Fig. 11, a noticeable correlation exists between  
 323 CaCO<sub>3</sub> production and phosphogypsum dosage. As phosphogypsum dosages increases, the  
 324 CaCO<sub>3</sub> content in the specimens cured through the stirring method increases from around 4% to  
 325 9%, and those cured through immersion increases from 5% to about 10%. In comparison, with the  
 326 same phosphogypsum dosage, the CaCO<sub>3</sub> content increases by approximately 25% when using the  
 327 immersion method compared to that when the stirring method is used. These findings are  
 328 consistent with existing studies, illustrating a direct linear correlation between CaCO<sub>3</sub> content and  
 329 the unconfined compressive strength of microbiologically cured specimens [31]. With the increase  
 330 in CaCO<sub>3</sub> content, there is an increase in the unconfined compressive strength. This highlights the  
 331 significance of CaCO<sub>3</sub> deposition, which directly influences the strength of the microbiologically  
 332 treated specimens, confirming its role as a key determinant in the effectiveness of MICP  
 333 technology [30].

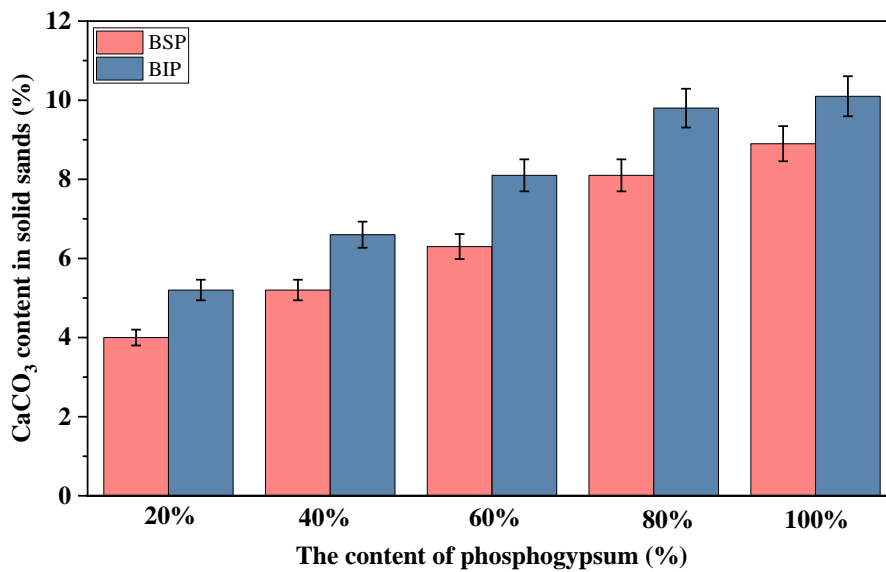


**Fig. 11.** CaCO<sub>3</sub> content in varied phosphogypsum dosages.

334 **3.4. Assessment of leached harmful elements**

335 Leaching of harmful elements from the phosphogypsum-cured specimens is studied in this  
 336 section, with the goal of assessing the environmental safety of MICPP and its benefits for eco-  
 337 friendly and sustainable development. Fig. 12 (a) illustrates the correlation between fluoride  
 338 content in the leachate of the sand columns and time. Additionally, Fig. 12 (b) presents the pH  
 339 values of the leachate. An important observation is the significant decrease in fluoride  
 340 concentration in the microbially cured sand columns, accounting for approximately 10% of the  
 341 pre-curing levels. This observation may be attributable to the microbial cell membranes that  
 342 harbor functional groups such as carboxyl and amino groups. The groups engage with ions via  
 343 diverse chemical bonds, encompassing hydrogen bonds, van der Waals forces, and ligand bonds.  
 344 These interactions play a pivotal role in the adsorption process. Metal ions or other multivalent  
 345 ions may serve as "bridging" ions linking microbial cell surfaces or biofilms to negatively charged  
 346 fluoride ions, thereby facilitating the indirect adsorption of fluoride. This phenomenon occurs via  
 347 the formation of ligand or alternative chemical bonds with both surfaces <sup>[58]</sup>. Furthermore, there  
 348 exists a potential for fluoride to be encapsulated within the calcium carbonate precipitate  
 349 generated during the MICPP reaction, leading to a substantial reduction in fluoride concentration  
 350 in the water.

351 The leachate from the microbially cured sand columns show higher pH values than the  
 352 leachate from uncured sand columns. After the microbial mineralization, the leachate approaches  
 353 to a nearly neutral pH, in contrast to the initially faster pH reduction observed in the leachate from  
 354 the uncured sand column, which shows a more acidic nature. According to the standard for  
 355 groundwater quality (GB/T 14848-2017) <sup>[59]</sup>, the fluoride concentration in the 60-day leachate

356 from the MICPP-treated sand column is 1.52 mg/L, surpasses the 1 mg/L standard for Class I  
 357 groundwater quality but still below the 2 mg/L standard for Class IV groundwater quality. Thus,  
 358 the leachate from the MICPP treated specimens is suitable for agriculture and certain industrial  
 359 water applications, implying potential suitability for domestic drinking water after further  
 360 treatment. The pH value of the 60-day leachate from the cured specimen falls within the Class I  
 361 groundwater quality range of 6.5-8.5, complying with the established standard. This affirms the  
 362 effective sequestration of harmful elements within phosphogypsum by microbial curing, thereby  
 363 reducing water contamination.

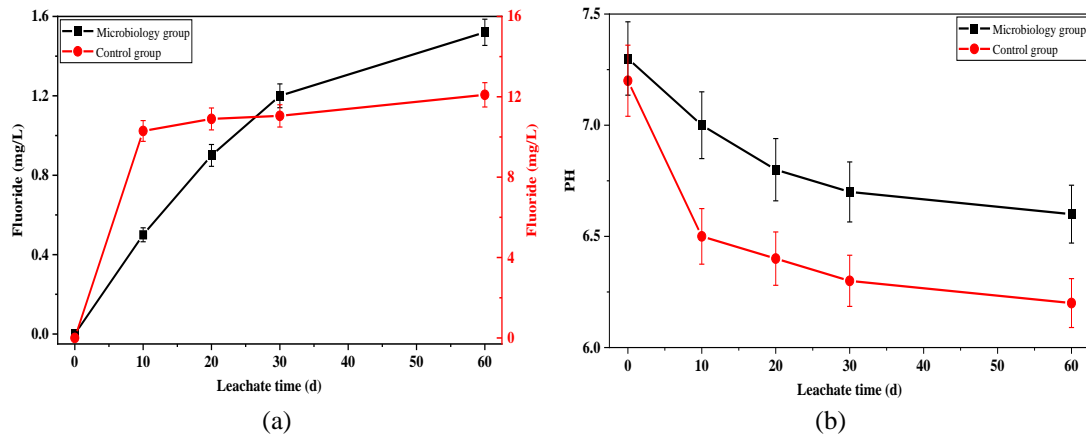
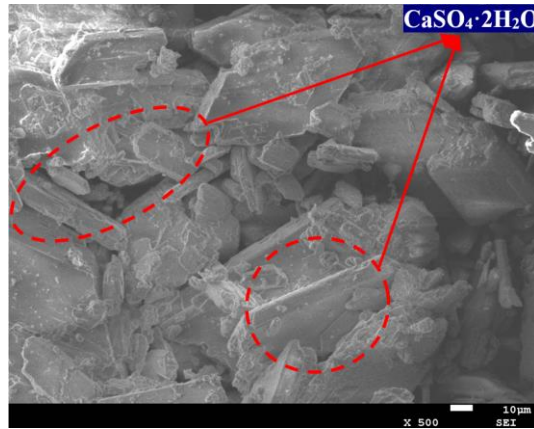


**Fig. 12.** Fluoride concentration change curve and pH change curve of leaching solution.

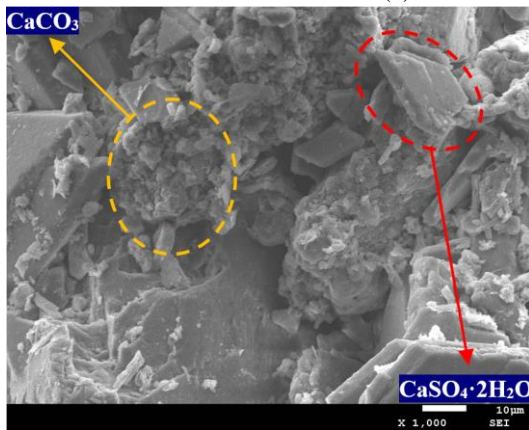
### 364 **3.5. Mechanistic analysis of MICPP**

365 SEM is employed to examine the micro-morphology of the untreated phosphogypsum and  
 366 MICPP-treated sand columns. A magnification of 500 is utilized to achieve a clearer crystal  
 367 morphology of the untreated phosphogypsum, while a magnification of 1000 is employed to  
 368 observe the micro-morphology of  $\text{CaCO}_3$  in the MICPP-treated sand columns. The micro-  
 369 morphology of the MICPP-treated sand columns is assessed under different curing conditions, as  
 370 illustrated in Fig. 13. The crystal morphology of  $\text{CaSO}_4 \cdot 2\text{H}_2\text{O}$  appears as tetragonal thin plates.  
 371 The MICPP treatment results in the deposition of  $\text{CaCO}_3$  precipitates, effectively filling the pores  
 372 within the specimen. The locally generated  $\text{CaCO}_3$  precipitates agglomerate in colloids of larger  
 373 particle size. With an increase in phosphogypsum, there is a proportional increase in the  $\text{CaCO}_3$   
 374 precipitates, leading to enhanced inter-crystal cementation. Consequently, pore space is reduced,  
 375 significantly improving the structural stability and cementation of the sand column. These  
 376 observations align with the results of the unconfined compressive strength tests, where the BIP  
 377 group outperforms the BSP group. The stirring method used in the BSP group may lead to an  
 378 uneven spatial distribution of reactants due to physical stirring limitations, thereby affecting  
 379 reaction homogeneity and adequacy. In contrast, the immersion method employed in the BIP

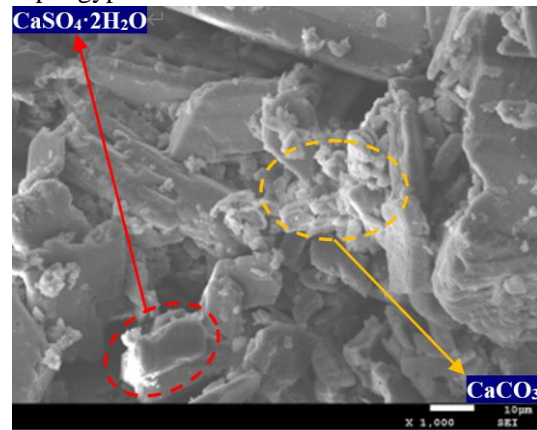
380 group allows for prolonged contact between the sand column and reactants, ensuring sufficient  
381 reaction time. The filling of pore and the bonding of sand grains are facilitated by calcium  
382 carbonate precipitation. This mechanism reduces microscopic defects, increases compactness, and  
383 enhances homogeneity, ultimately improving the overall structural integrity of the sand columns.



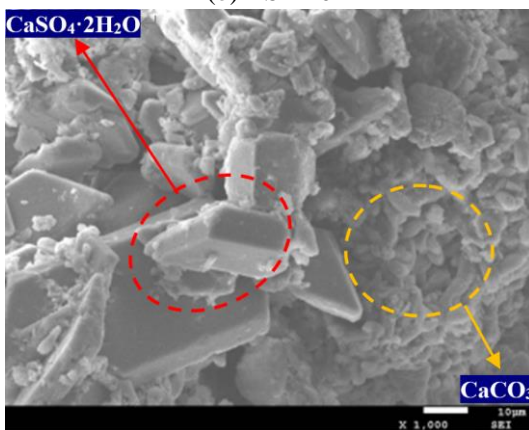
(a) Untreated phosphogypsum



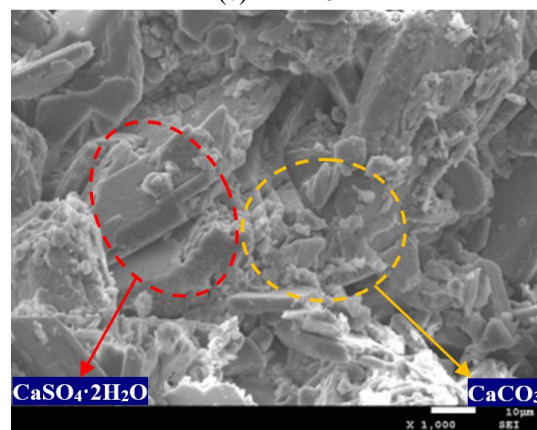
(b) BSP-20



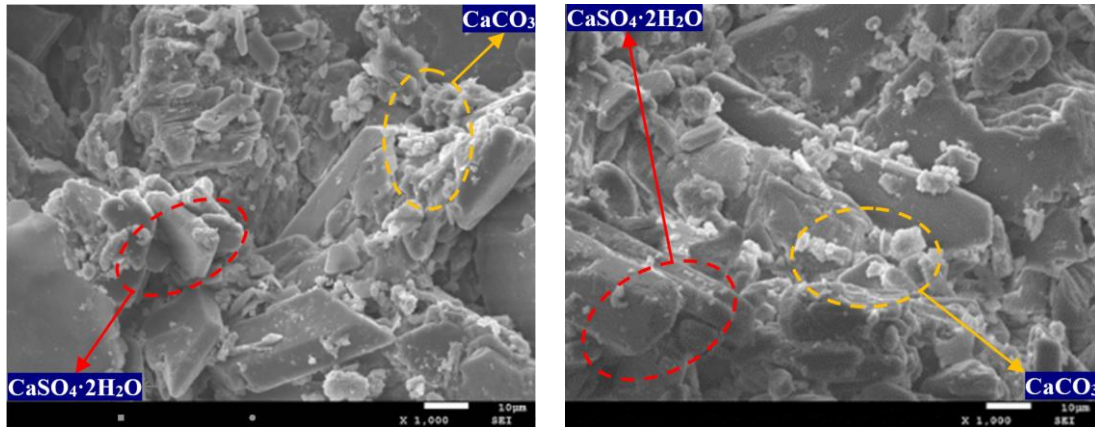
(c) BIP-20



(d) BSP-60



(e) BIP-60



(f) BSP-100

(g) BIP-100

384 **Fig. 13.** SEM micromorphology of untreated phosphogypsum and sand columns treated with  
 385 MICPP.

386 To provide further clarity on the mineralization mechanism induced by MICPP in the  
 387 phosphogypsum, XRD tests are conducted to compare the composition of the samples undergoing  
 388 microbial-induced mineralization with those not exposed to the microbes. The XRD results of the  
 389 sand columns with different phosphogypsum dosages before and after MICPP treatment are  
 390 illustrated in Fig. 14, wherein the XRD analyses of the sterile fluid samples show two primary  
 391 phases, i.e.,  $\text{SiO}_2$  and  $\text{CaSO}_4 \cdot 2\text{H}_2\text{O}$ . This aligns with the expectations, as silica is the primary  
 392 constituent of sand and calcium sulfate dihydrate is the principal component of phosphogypsum.  
 393 In the specimens exposed to microbial influence, in addition to the expected  $\text{SiO}_2$  phase, new  
 394 mineral phases are observed, characterized by the distinctive absorption peaks of calcite ( $\text{CaCO}_3$ ).  
 395 The experimental results demonstrate that the precipitated  $\text{CaCO}_3$  primarily takes on a crystalline  
 396 form known as calcite that is characterized by a stable crystal structure and high resistance to  
 397 solubility, signifies durability and long-lasting maintenance of morphology, as it is resistant to  
 398 dissolution or decomposition under various conditions. Additionally, calcite enhances the strength  
 399 of the sand columns. The analysis of the XRD results of sand columns with different  
 400 phosphogypsum dosages shows that the  $\text{CaSO}_4 \cdot 2\text{H}_2\text{O}$  phase is almost absent at 80%  
 401 phosphogypsum dosage, whereas at other phosphogypsum dosages, the  $\text{CaSO}_4 \cdot 2\text{H}_2\text{O}$  phase is still  
 402 present. This finding suggests that the conversion from  $\text{CaSO}_4 \cdot 2\text{H}_2\text{O}$  to  $\text{CaCO}_3$  in the MICPP  
 403 treatment is more efficient at 80% phosphogypsum dosage. This discovery aligns with the results  
 404 above concerning both the unconfined compressive strength and the permeability coefficient.

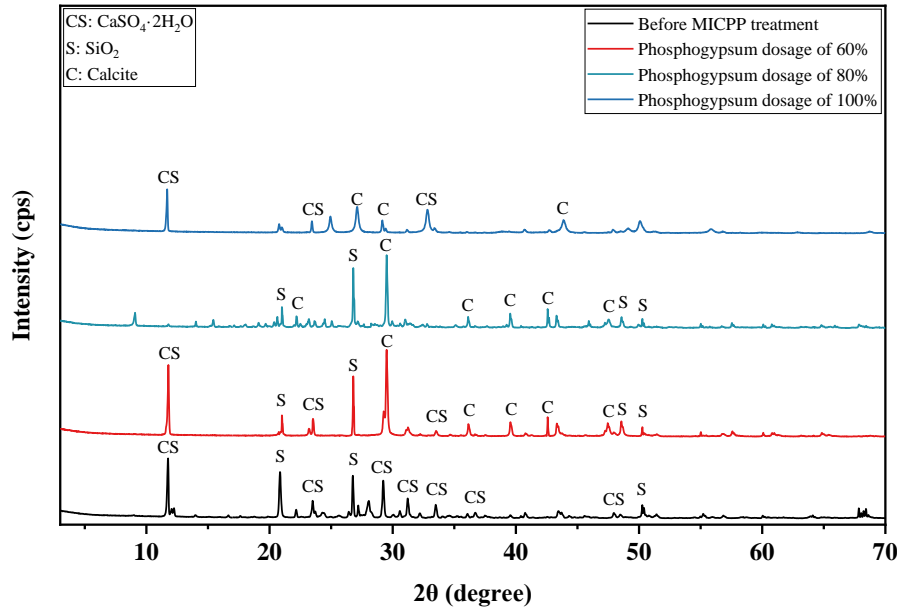


**Fig. 14.** X-ray diffractograms of sand columns with different amount of phosphogypsum before and after MICPP treatment.

405 Bacillus pasteurus is employed in the experiments of the MICPP process. These  
 406 microorganisms act as catalysts, triggering the decomposition of urea—a fundamental process in the  
 407 mineralization reactions of MICPP. The MICPP mineralization reaction comprises two primary  
 408 steps: urea hydrolysis and  $\text{CaCO}_3$  precipitation. As shown in Fig. 15. Stage I: The initial step  
 409 involves the action of urease, catalyzing the breakdown of urea ( $\text{NH}_2\text{CONH}_2$ ) into ammonium  
 410 ions ( $\text{NH}_4^+$ ) and carbonate ions ( $\text{CO}_3^{2-}$ ). The continued accumulation of  $\text{NH}_4^+$  and  $\text{CO}_3^{2-}$  increases  
 411 the cellular membrane potential and raises the overall pH of the solution. This alkaline  
 412 environment encourages the continuous accumulation of  $\text{NH}_4^+$  and  $\text{CO}_3^{2-}$ . Simultaneously, urease  
 413 is produced through the metabolism of Bacillus pasteurianus, and extracellular polymers are  
 414 produced [60]. Stage II: The polymers, combined with the double-layer structure of  
 415 microorganisms, tend to adhere to the surfaces of the sand particles. Functional groups such as  
 416 hydroxyl, amine, amide, carboxyl, etc. present on the surface of microbial cell membranes carry  
 417 negative charges.  $\text{Ca}^{2+}$  released from the phosphogypsum is attracted to this negatively charged  
 418 surface, leading to substantial  $\text{Ca}^{2+}$  accumulation on the cell surface. Concurrently,  $\text{CO}_3^{2-}$   
 419 produced through urea hydrolysis is transported extracellularly. The convergence of  $\text{Ca}^{2+}$  and  
 420  $\text{CO}_3^{2-}$  at the cell serves as a nucleation site, initiating the gradual formation of  $\text{CaCO}_3$  crystals [61].  
 421 As these crystals develop, the microbial bacteria become completely encased by them, restricting  
 422 nutrient transport and ultimately leading to the demise of the bacteria. Typically, higher specimen  
 423 strength is associated with the increased  $\text{CaCO}_3$  content in the specimen. However, strength also  
 424 depends on the distribution and form of  $\text{CaCO}_3$  cementation. Cementation is classified into three

425 categories based on the relationship between  $\text{CaCO}_3$  and particle size [62]: (1) Coating Role:  
 426  $\text{CaCO}_3$  covers particle surfaces, enhancing particle volume and surface area without interparticle  
 427 contact. (2) Bonding Role:  $\text{CaCO}_3$  primarily resides near particle contact points, causing  
 428 aggregation and bonding between particles. (3) Bridging Role:  $\text{CaCO}_3$  accumulates between  
 429 adjacent particles without direct contact, fostering growth until the particles contact each other.  
 430 These forms of  $\text{CaCO}_3$  cementation enhance specimen strength and reduce permeability. However,  
 431 structural improvement primarily depends on the bonding and bridging roles of  $\text{CaCO}_3$ .

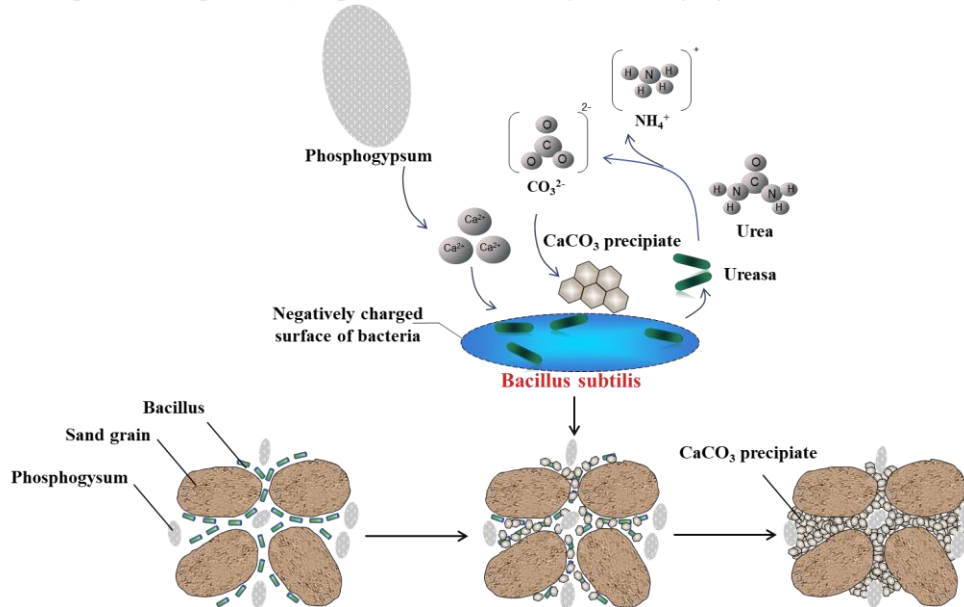


**Fig. 15.** Schematic diagram of the principle of microbial-induced  $\text{CaCO}_3$  precipitation using phosphogypsum.

#### 432 4. Conclusions

433 In this paper, the MICPP technology is introduced and implemented for the treatment of sand  
 434 using phosphogypsum as the calcium source. Subsequently, the performance and mechanism of  
 435 the treated sand columns are analyzed and evaluated, and the conclusions drawn can be  
 436 summarized as follows:

437 (1) In the process of MICPP, bacterial and nutrient solutions permeate the pores between the  
 438 particles. This facilitates hydrolysis of urease, interacting with the free calcium ions extracted  
 439 from phosphogypsum, thereby initiating the formation of  $\text{CaCO}_3$  crystals. The resultant crystals  
 440 contribute to enhancing the density and uniformity of the sand by bonding the particles together  
 441 and filling the pores, consequently fortifying the overall structural integrity of the sand.

442 (2) On a macroscopic scale, MICPP strengthens specimens. A higher phosphogypsum  
 443 dosage is associated with an elevated unconfined compressive strength and a decreased

444 permeability coefficient. The permeability coefficient of the MICPP-treated specimens is ten times  
445 lower than that of the untreated specimens. Remarkably, the immersion method exhibits superior  
446 curing efficiency when compared with the stirring method.

447 (3) The leachate from the control group, where phosphogypsum is cured without microbial  
448 treatment, surpasses applicable emission standards. In contrast, harmful leaching tests conducted  
449 on the leachate of the sand columns show that the MICPP process reduces environmental  
450 contaminability.

451 (4) On a microscopic scale, the increased strength is associated with the expanded pores  
452 filled with  $\text{CaCO}_3$ . Microbially induced calcium precipitation predominantly encompasses calcite,  
453 providing robust stability and serving as a bonding and bridging agent.

#### 454 **Acknowledgement**

455 The authors are grateful for the financial support from the National Natural Science  
456 Foundation of China (Grant No.52308266), the Programme of Introducing Talents of Discipline to  
457 Universities (i.e., the 111 Project of China, Grant No. D20015), and the 111 Project of Hubei  
458 Province (Grant No. 2021EJD026).

#### 459 **References**

- 460 [1] Cayan, D. R., Bromirski, P. D., Hayhoe, K., et al. (2007). Climate change projections of sea level  
461 extremes along the California coast. *Climatic Change*, 87(1 SUPPL), S57-S73.
- 462 [2] Chu, J., Ivanov, V., He, J., et al. (2011). Development of microbial geotechnology in Singapore.  
463 *American Society of Civil Engineers (ASCE)*, 211, 4070-4078.
- 464 [3] DeJong, J. T., Mortensen, B. M., Martinez, B. C., et al. (2010). Bio-mediated soil improvement.  
465 *Ecological Engineering*, 36(2), 197-210.
- 466 [4] Benhelal, E., Zahedi, G., Shamsaei, E., et al. (2013). Global strategies and potentials to curb  $\text{CO}_2$   
467 emissions in cement industry. *Journal of Cleaner Production*, 51, 142-161.
- 468 [5] P, S. (1993). *Soil stabilization with cement and lime: State of the art review*. London: Her  
469 Majesty's Stationery Office.
- 470 [6] Huntzinger, D. N., Eatmon, T. D. (2009). A life-cycle assessment of Portland cement  
471 manufacturing: comparing the traditional process with alternative technologies. *Journal of*  
472 *Cleaner Production*, 17(7), 668-675.
- 473 [7] Meyer, C. (2009). The greening of the concrete industry. *Cement & Concrete Composites*, 31(8),  
474 601-605.
- 475 [8] Wang, B., Yan, L., Fu, Q., et al. (2021). A Comprehensive Review on Recycled Aggregate and  
476 Recycled Aggregate Concrete. *Resource Conservation and Recycling*, 171, 105565.
- 477 [9] DeJong, J. T., Fritzges, M. B., Nusslein, K. (2006). Microbially induced cementation to control  
478 sand response to undrained shear. *Journal of Geotechnical and Geoenvironmental Engineering*,  
479 132(11), 1381-1392.
- 480 [10] Sun, X., Miao, L., Tong, T., et al. (2018). Improvement of Microbial-Induced Calcium Carbonate  
481 Precipitation Technology for Sand Solidification. *Journal of Materials in Civil Engineering*,  
482 30(11), 04018301.

- 483 [11] Sun, Xiao-Hao, Miao, Lin-Chang, Tong, Tian-Zhi. (2018). Effect of methods of adding urea in  
484 culture media on sand solidification tests. *Yantu Gongcheng Xuebao/Chinese Journal of*  
485 *Geotechnical Engineering*, 40(5), 939-944. (in Chinese)
- 486 [12] Dejong, J. T., Soga, K., Kavazanjian, E., et al. (2013). Biogeochemical processes and  
487 geotechnical applications: Progress, opportunities and challenges. *Geotechnique*, 63(4), 287-301.
- 488 [13] Al-Salloum, Y., Hadi, S., Abbas, H., et al. (2017). Bio-induction and bioremediation of  
489 cementitious composites using microbial mineral precipitation - A review. *Construction and*  
490 *Building Materials*, 154, 857-876.
- 491 [14] Umar, M., Kassim, K. A., Ping Chiet, K. T. (2016). Biological process of soil improvement in  
492 civil engineering: A review. *Journal of Rock Mechanics and Geotechnical Engineering*, 8(5), 767-  
493 774.
- 494 [15] Martinez, B. C., DeJong, J. T., Ginn, T. R., et al. (2013). Experimental Optimization of Microbial-  
495 Induced Carbonate Precipitation for Soil Improvement. *Journal of Geotechnical and*  
496 *Geoenvironmental Engineering*, 139(4), 587-598.
- 497 [16] Qian, C. X., Wang, R. X., Cheng, L. A., et al. (2010). Theory of Microbial Carbonate  
498 Precipitation and Its Application in Restoration of Cement-based Materials Defects. *Chinese*  
499 *Journal of Chemistry*, 28(5), 847-857. (in Chinese)
- 500 [17] Ruan, S., Qiu, J., Weng, Y., et al. (2019). The use of microbial induced carbonate precipitation in  
501 healing cracks within reactive magnesia cement-based blends. *Cement and Concrete Research*,  
502 115, 176-188.
- 503 [18] Choi, S., Wang, K., Wen, Z., et al. (2017). Mortar crack repair using microbial induced calcite  
504 precipitation method. *Cement and Concrete Composites*, 83, 209-221.
- 505 [19] Son, H., Kim, H., Park, S., et al. (2018). Ureolytic/Non-Ureolytic Bacteria Co-Cultured Self-  
506 Healing Agent for Cementitious Materials Crack Repair. *Materials*, 11(5), 782.
- 507 [20] Mwandira, W., Nakashima, K., Kawasaki, S. (2017). Bioremediation of lead-contaminated mine  
508 waste by *Pararhodobacter* sp. based on the microbially induced calcium carbonate precipitation  
509 technique and its effects on strength of coarse and fine grained sand. *Ecological Engineering*, 109,  
510 57-64.
- 511 [21] Kang, C., Oh, S. J., Shin, Y., et al. (2015). Bioremediation of lead by ureolytic bacteria isolated  
512 from soil at abandoned metal mines in South Korea. *Ecological Engineering*, 74, 402-407.
- 513 [22] Simatupang, M., & Okamura, M. (2017). Liquefaction resistance of sand remediated with  
514 carbonate precipitation at different degrees of saturation during curing. *Soils and Foundations*,  
515 57(4), 619-631.
- 516 [23] Montoya, B. M., Dejong, J. T., & Boulanger, R. W. (2013). Dynamic response of liquefiable sand  
517 improved by microbial-induced calcite precipitation. *Geotechnique*, 63(4), 302-312.
- 518 [24] Wang, Z., Zhang, N., Ding, J., et al. (2018). Experimental Study on Wind Erosion Resistance and  
519 Strength of Sands Treated with Microbial-Induced Calcium Carbonate Precipitation. *Advances in*  
520 *Materials Science & Engineering*, 3463298.
- 521 [25] Whiffin, V. S. (2004). Microbial CaCO<sub>3</sub> precipitation for the production of biocement. Murdoch  
522 University.
- 523 [26] Castro-Alonso, M. J., Montañez-Hernandez, L. E., Sanchez-Muñoz, M. A., et al. (2019).  
524 Microbially Induced Calcium Carbonate Precipitation (MICP) and its Potential in Bioconcrete:  
525 Microbiological and Molecular Concepts. *Frontiers in Materials*, 126, 1-15.
- 526 [27] De Muynck, W., De Belie, N., & Verstraete, W. (2010). Microbial carbonate precipitation in

- 527 construction materials: A review. *Ecological Engineering*, 36(2), 118-136.
- 528 [28] Harkes, M. P., Booster, J. L., Paassen, L. A. V., & Loosdrecht, M. C. M. V. (2008). Microbial  
529 induced carbonate precipitation as ground improvement method - Bacterial fixation and empirical  
530 correlation  $\text{CaCO}_3$  vs strength. 1st International Conference on Bio-Geo-Civil Engineering.
- 531 [29] Chu, J., Ivanov, V., Naeimi, M., et al. (2014). Optimization of calcium-based bioclogging and  
532 biocementation of sand. *Acta Geotechnica*, 9(2), 277-285.
- 533 [30] Whiffin, V. S., van Paassen, L. A., & Harkes, M. P. (2007). Microbial Carbonate Precipitation as  
534 a Soil Improvement Technique. *Geomicrobiology Journal*, 24(5), 417-423.
- 535 [31] Chou, C., Seagren, E. A., Aydilek, A. H., et al. (2011). Biocalcification of Sand through Ureolysis.  
536 *Journal of Geotechnical and Geoenvironmental Engineering*, 137(12), 1179-1189.
- 537 [32] Bing, L. (2014). Geotechnical properties of biocement treated soils. Singapore: Nanyang  
538 Technological University.
- 539 [33] Ferris, F. G., Stehmeier, L. G., Kantzas, A., & Mourits, F. M. (1996). Bacteriogenic mineral  
540 plugging. *J Can Pet Technol*, 35(08), 56-61.
- 541 [34] Chu, J., Ivanov, V., Stabnikov, V., et al. (2013). Microbial method for construction of an  
542 aquaculture pond in sand. *Géotechnique*, 63(10), 871-875.
- 543 [35] Vijay, K., & Murmu, M. (2019). Effect of calcium lactate on compressive strength and self-  
544 healing of cracks in microbial concrete. *Frontiers of Structural and Civil Engineering*, 13(3), 515-  
545 525.
- 546 [36] Hammes, F., Boon, N., de Villiers, J., et al. (2003). Strain-Specific Ureolytic Microbial Calcium  
547 Carbonate Precipitation. *Applied and Environmental Microbiology*, 69(8), 4901-4909.
- 548 [37] Gorospe, C. M., Han, S., Kim, S., et al. (2013). Effects of different calcium salts on calcium  
549 carbonate crystal formation by *Sporosarcina pasteurii* KCTC 3558. *Biotechnology and  
550 Bioprocess Engineering*, 18(5), 903-908.
- 551 [38] Casas, C. C., Schaschke, C. J., Akunna, J. C., et al. (2019). Dissolution experiments on dolerite  
552 quarry fines at low liquid-to-solid ratio: a source of calcium for MICP. *Environmental  
553 Geotechnics*, 9(6), 331-339.
- 554 [39] Nedelciu, C. E., Ragnarsdottir, K. V., Schlyter, P., et al. (2020). Global phosphorus supply chain  
555 dynamics: Assessing regional impact to 2050. *Global Food Security*, 26, 100426.
- 556 [40] Rashad, A. M. (2017). Phosphogypsum as a construction material. *Journal of Cleaner Production*,  
557 166, 732-743.
- 558 [41] Sahu, S. K., Ajmal, P. Y., Bhangare, R. C., et al. (2014). Natural radioactivity assessment of a  
559 phosphate fertilizer plant area. *Journal of Radiation Research and Applied Sciences*, 7(1), 123-  
560 128.
- 561 [42] Zirnea, S., Lazar, I., Foudjo, B. U. S., et al. (2013). Cluster Analysis Based of Geochemical  
562 Properties of Phosphogypsum Dump Located Near Bacau City in Romania. *APCBEE Procedia*, 5,  
563 317-322.
- 564 [43] Cárdenas-Escudero, C., Morales-Flórez, V., Pérez-López, R., et al. (2011). Procedure to use  
565 phosphogypsum industrial waste for mineral  $\text{CO}_2$  sequestration. *Journal of Hazardous Materials*,  
566 196, 431-435.
- 567 [44] Yin, T., Yang, R., Du, J., et al. (2019). Effects of acid and phosphate on arsenic solidification in a  
568 phosphogypsum-based cement backfill process. *RSC Advances*, 9(48), 28095-28101.
- 569 [45] Sun, X., Miao, L., Wu, L., et al. (2019). Improvement of bio-cementation at low temperature  
570 based on *Bacillus megaterium*. *Applied Microbiology and Biotechnology*, 103(17), 7191-7202.

- 571 [46] Song yu, L., & Ke gong, Z. (2010). Soil mechanics. China Architecture & Building Press. (in  
572 Chinese)
- 573 [47] Yahui, Y., Gang, X., & Bin, T. (2021). Carbonation characteristics of cement-based materials  
574 under the uniform distribution of pore water. *Construction and Building Materials*, 275, 121450.
- 575 [48] China National Environmental Protection Standards. (2020). HJ 1147-2020, Water quality  
576 Determination of pH-Electrode method. (in Chinese)
- 577 [49] China National Standards. (1987). GB/T 7484-1987, Water quality Determination of fluoride-Ion  
578 selective electrode method. (in Chinese)
- 579 [50] Choi, S.-G., Chang, I., Lee, M., Lee, J.-H., Han, J.-T., Kwon, T.-H. (2020). Review on  
580 geotechnical engineering properties of sands treated by microbially induced calcium carbonate  
581 precipitation (MICP) and biopolymers. *Construction and Building Materials*, 246, 118415.
- 582 [51] Qabany, A. A., & Soga, K. (2013). Effect of chemical treatment used in MICP on engineering  
583 properties of cemented soils. *Geotechnique*, 63(4), 331-339.
- 584 [52] L. Cheng, R. Cord-Ruwisch, M.A. Shahin, (2013). Cementation of sand soil by microbially  
585 induced calcite precipitation at various degrees of saturation, *Can. Geotech. J.* 50(1), 81-90.
- 586 [53] Zhao, Q., Li, L., Li, C., et al. (2014). Factors Affecting Improvement of Engineering Properties of  
587 MICP-Treated Soil Catalyzed by Bacteria and Urease. *Journal of Materials in Civil Engineering*,  
588 26(12), 4014094.
- 589 [54] Cheng, L., Shahin, M. A., & Mujah, D. (2017). Influence of Key Environmental Conditions on  
590 Microbially Induced Cementation for Soil Stabilization. *Journal of Geotechnical and  
591 Geoenvironmental Engineering*, 143(1), 04016083.
- 592 [55] Li, M., Wen, K., Li, Y., et al. (2018). Impact of Oxygen Availability on Microbially Induced  
593 Calcite Precipitation (MICP) Treatment. *Geomicrobiology Journal*, 35(1), 15-22.
- 594 [56] S.-G. Choi, K. Wang, J. Chu, (2016). Properties of biocemented, fiber reinforced sand, *Constr.*  
595 *Build. Mater.* 120, 623-629.
- 596 [57] A. Zamani, B.M. Montoya, (2017). Shearing and hydraulic behavior of MICP treated silty sand,  
597 *Geotechnical Frontiers*, 290-299.
- 598 [58] Burns, J. L. , Ginn, B. R. , Bates, D. J. , Dublin, S. N. , Taylor, I. V. , & Apkarian, R. P. , et al.  
599 (2010). Outer membrane-associated serine protease involved in adhesion of shewanella  
600 oneidensis to Fe(III) Oxides. *Environmental Science & Technology*, 44(1), 68-73.
- 601 [59] China National Standards. (2017). GB/T 14848-2017, Standard for groundwater quality. (in  
602 Chinese)
- 603 [60] Dick, J., De Windt, W., De Graef, B., et al. (2006). Bio-deposition of a calcium carbonate layer  
604 on degraded limestone by *Bacillus* species. *Biodegradation*, 17(4), 357-367.
- 605 [61] Dhimi, N. K., Reddy, M. S., & Mukherjee, A. (2013). Biomineralization of calcium carbonates  
606 and their engineered applications: a review. *Frontiers in Microbiology*, 4, 1-13.
- 607 [62] Lin, H., Suleiman, M. T., & Brown, D. G. (2020). Investigation of pore-scale CaCO<sub>3</sub> distributions  
608 and their effects on stiffness and permeability of sands treated by microbially induced carbonate  
609 precipitation (MICP). *Soils and Foundations*, 60(4), 944-961.